Dynamic elements of chaos in the Willamowski–Rössler network

Baltazar D. Aguda and Bruce L. Clarke

Citation: The Journal of Chemical Physics **89**, 7428 (1988); doi: 10.1063/1.455272
View online: http://dx.doi.org/10.1063/1.455272
View Table of Contents: http://scitation.aip.org/content/aip/journal/jcp/89/12?ver=pdfcov
Published by the AIP Publishing

Dynamic elements of chaos in the Willamowski–Rössler network

Baltazar D. Aguda[a] and Bruce L. Clarke
Department of Chemistry, University of Alberta, Edmonton, Alberta T6G 2G2, Canada

(Received 1 August 1988; accepted 6 September 1988)

Two dynamic elements of the Willamowski–Rössler network are identified: one of which is a Lotka–Volterra oscillator involving two autocatalytic species X and Y, while the other is a switch between X and a third autocatalytic species Z. These two dynamic elements are coupled via X. Nonperiodic oscillations arise only if X autocatalyzes faster than Z. The chaotic nature of the oscillations is confirmed using the Shil'nikov theorem which requires the existence of a homoclinic orbit doubly asymptotic to a steady state of the saddle-focus type. Under chaotic conditions, two steady states coexist inside the positive orthant of concentration space and both satisfy the conditions of the Shil'nikov theorem. Chaos is further shown by the existence of several unstable period-3 fixed points of first-return Poincaré maps. A chaotic attractor is found and its changing structure under various sets of parameters is established.

I. INTRODUCTION

Prototype model mechanisms are now available for many of the nonlinear behavior observed in various experimental reaction systems. These are models with a minimal number of reactions and species, and which almost exclusively exhibit any one of the dynamical phenomena such as hysteresis between branches of stable steady states, damped or sustained oscillations and even chaos. Sometimes large reaction networks exhibiting different dynamics under various conditions are built simply from a combination of these minimal models. In this case we refer to these minimal models as the *dynamic elements* of the network. An intuitive understanding of the complex dynamics of large reaction networks can be achieved when these dynamic elements are identified and their interaction fully understood. Conversely, once we have a catalog of dynamic elements and have worked out the resultant behavior when these are coupled, it will be possible to design networks with any desired behavior.

An example of a dynamic element is the simple damped oscillator given by Lotka[1] in 1910. Lotka's network involves two species, one of them autocatalytic. In an analysis of Olsen's model for the peroxidase–oxidase reaction,[2] it has been shown[3] that the complex oscillations can be understood by considering the coupling of two positive feedback loops, one of which is the Lotka damped oscillator.

Another dynamic element is the Lotka–Volterra[4] network which generates sustained oscillations. This network has two autocatalytic species that are involved in three reactions. This oscillator, however, is unfit to model realistic chemical oscillators because it is structurally unstable. In contrast, the two-species trimolecular model called the Brusselator[5] can be taken as a model for limit cycle oscillations. Several others have also been discovered or designed. Coupling of two of these oscillatory dynamic elements sometimes results in birhythmicity,[6] a condition in which the system has two stable oscillatory states coexisting under the same parameter values.

One practical significance of being able to identify the essential dynamic elements of a reaction network is demonstrated by the success of the recipe that Epstein and coworkers[7] have employed to design several chemical oscillators in the laboratory. This recipe has two essential ingredients—one is a bistable network and the other is a feedback that switches the system between the two stable branches of the bistable component. The resulting oscillatory network exhibits what is now popularly known as the cross-shaped phase diagram.[7]

Modeling static instabilities of complex mechanisms has also benefited from a familiarity of the essential feedback loops present in prototype models. For instance, our previous work[8] on the peroxidase–oxidase network showed that two feedback cycles—namely, a catalytic cycle and an inhibition cycle—are necessary for bistability in this system. This conclusion was derived from an analysis of the much simpler classical enzyme substrate-inhibition mechanism.[9] An efficient method of identifying these *static elements* is a key result of the formalism called stoichiometric network analysis (SNA) developed by Clarke.[10] These elements are what he calls *extreme currents*.

The design of chaotic oscillators can be said to have been started more than a decade ago by Rössler[11] when he first introduced his *reinjection principle*. This principle requires that the trajectorial flow consists of an oscillation between two species and that the oscillations are "molded" on an S-shaped slow manifold formed from the dynamics of a third variable. Oscillation around an unstable focus, for example, on one stable branch of the slow manifold reaches a certain threshold at which the trajectories jump to the other stable branch with a different orientation of the flow and then part of this flow gets "reinjected" into the first branch. Thus, if one couples an Edelstein switch and a Turing oscillator, chaotic oscillations are observed if the right parameter values are chosen.[11] "Spiral-type" chaos is generated by these two components. Another type of chaos, the "screw-type," was designed by Rössler[12] using the hysteresis between two stable limit cycles. Several abstract reaction systems capable of chaos have also been constructed using these basic components.[11,12]

This paper presents a detailed analysis of the Willamowski–Rössler model,[13] a three-species network that ex-

[a] Present address: Department of Chemistry, Indiana University–Purdue University at Indianapolis, Indianapolis, Indiana 46223.

 0021-9606/88/247428-27$02.10

hibits complex oscillations under certain parameter values. This model is the first evidence that deterministic chaos can be generated by a chemically realistic mechanism. Surprisingly, no detailed analysis of the model has been reported that would further illuminate the source of chaos in the mechanism. In this paper, we show that one could understand the behavior of this system by considering how the two dynamic elements—a Lotka–Volterra oscillator and a switch—interact and generate nonperiodic oscillations under appropriate coupling. Section II gives a discussion of the mechanism and shows the behavior of the separate dynamic elements just mentioned. Section III presents our detailed numerical studies of the model showing how the dynamics change under varying coupling strength between the two elements, and that chaos is approached via period doubling. A full picture of the chaotic attractor is given along with the interesting changes in its structure as some parameters are varied. Section IV gives a proof of the chaotic nature of the oscillations invoking a theorem due to Shil'nikov[14] which requires the existence of homoclinic orbits doubly asymptotic to unstable steady states of the saddle-focus type. A discussion of the relevance of codimension-two bifurcation points as a diagnostic aid for chaos is included in the last section.

II. THE WILLAMOWSKI–RÖSSLER NETWORK

Willamowski and Rössler[13] were the first to show that deterministic chaos can be generated by a realistic chemical mechanism when they gave the following set of reactions that are at most bimolecular and the kinetics is mass action:

$$A_1 + X \underset{-1}{\overset{1}{\rightleftarrows}} 2X, \tag{R1}$$

$$X + Y \underset{-2}{\overset{2}{\rightleftarrows}} 2Y, \tag{R2}$$

$$A_5 + Y \underset{-3}{\overset{3}{\rightleftarrows}} A_2, \tag{R3}$$

$$X + Z \underset{-4}{\overset{4}{\rightleftarrows}} A_3, \tag{R4}$$

$$A_4 + Z \underset{-5}{\overset{5}{\rightleftarrows}} 2Z. \tag{R5}$$

Let the concentrations of $A_1, \ldots, A_5$ be held constant and thereby assume an open system. We now consider only the dynamics of the intermediates X, Y, and Z. Figure 1 shows the reaction network diagram involving these intermediates (the reverse reactions are not shown but are considered in all analyses below except when explicitly mentioned otherwise). The evolution of the concentrations x, y, and z under isothermal, constant volume, and spatially homogeneous conditions can be described by the following set of autonomous ordinary differential equations:

$$\begin{aligned} \dot{x} &= k_1 x - k_{-1} x^2 - k_2 xy + k_{-2} y^2 - k_4 xz + k_{-4}, \\ \dot{y} &= k_2 xy - k_{-2} y^2 - k_3 y + k_{-3}, \\ \dot{z} &= -k_4 xz + k_{-4} + k_5 z - k_{-5} z^2, \end{aligned} \tag{1}$$

where the constants A_i are already incorporated into the rate constants k_1, k_3, k_{-3}, k_{-4}, and k_5.

One recognizes from Fig. 1 the Lotka–Volterra (LV) oscillator involving autocatalytic species X and Y. This LV oscillator is coupled (via X) to an element called a "switch" between the autocatalytic species Z and X.

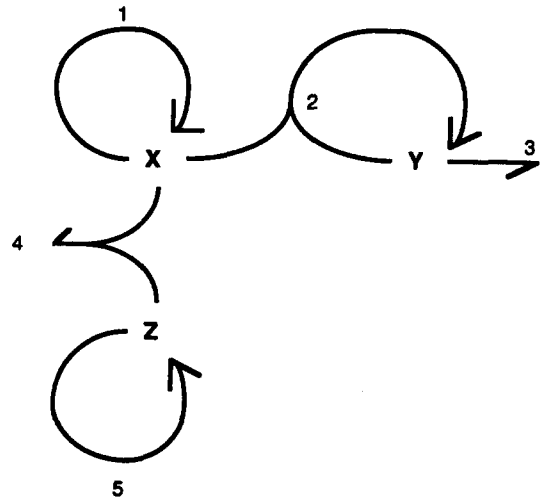

FIG. 1. Reaction network diagram of the Willamowski–Rössler (WR) model involving the dynamical species X, Y, and Z. All reactions are reversible and the network follows mass-action kinetics.

Figure 2 shows an example of the complex oscillations exhibited by the network under the given parameter values. The nonperiodic oscillations shown were started from a single initial condition. The two-dimensional projections of the trajectories [Figs. 2(a) and 2(b)] demonstrate the influence of the LV oscillator and switch elements on the dynamics of the full network. The LV oscillator (reactions 1, 2, and 3 without their reverse) has structurally unstable oscillations. With the introduction of the reverse of reactions 1, 2, and 3 these marginally stable oscillations collapse into damped oscillations as shown in Fig. 3(a).

The influence of the switch is clearly shown in Fig. 2(a). Switches generally lead to explosion of one species at the expense of another's extinction. The hyperbolic envelope in Fig. 2(a) demonstrates the intermittent explosion/extinction of species X and Z. The oscillations seen inside the envelope in Fig. 2(a) show the effect of the LV oscillator. In Fig. 3(b), the dynamics of the switch (reactions 1, 4, and 5 with their reverse) is shown. Using the same parameters that give nonperiodic oscillations for the full network (Fig. 2), we found three steady states for the switch element—one in which Z is almost extinct, another where X almost vanishes, and the third is an intermediate saddle point that separates the other two steady states [see Fig. 3(b)]. Notice the hyperbolic manifold to which trajectories from different initial conditions converge on their way to the stable steady state with low Z.

The right coupling between the LV and switch elements leads to the observed oscillations of the full system. This coupling can best be studied by varying k_4 and k_2. With k_4 large, we expect that the switch turns off either species X or species Z depending on the values of k_1 and k_5. Thus we must require that $k_1 > k_5$ to avoid the LV element of the network becoming extinct. By changing k_2, we vary the amplitude of the LV oscillation and vary the length of time given to the autocatalysis of X and Z whose concentrations are crucial to

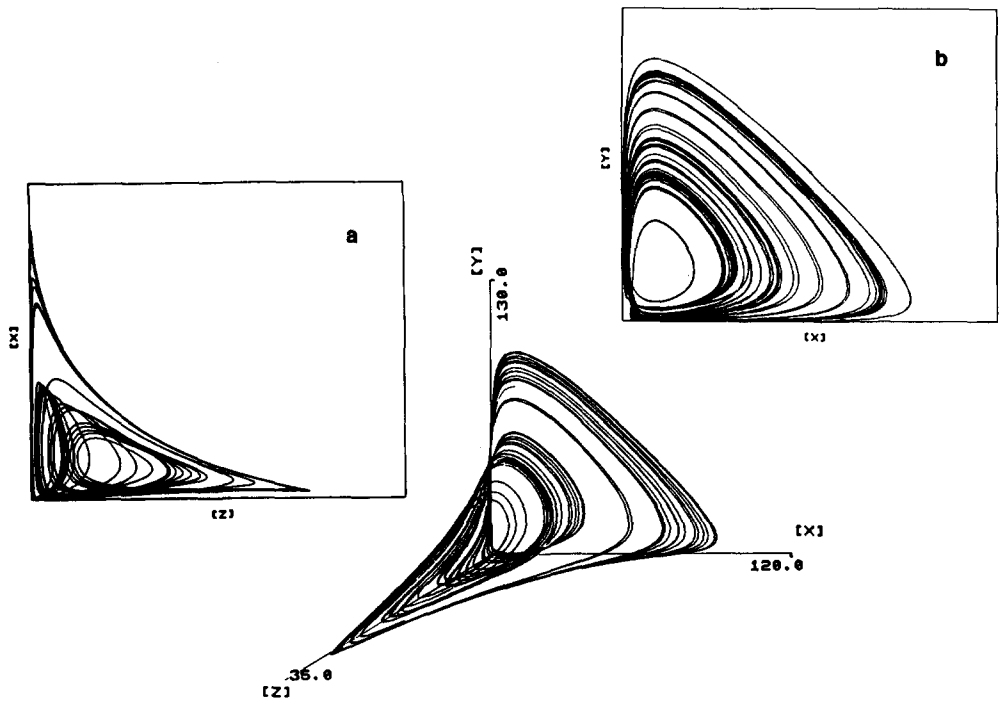

FIG. 2. Nonperiodic oscillations of the WR model started from a single initial condition. (a) Projection of the trajectories on the X–Z plane. The hyperbolic envelope (explosion/extinction tendency) of the trajectories demonstrates the influence of the switch element of the network. (b) Projection of the trajectories on the X–Y plane which shows the influence of the Lotka–Volterra (LV) oscillator element. Parameter values are: $k_1 = 30.0$, $k_{-1} = 0.25$, $k_2 = 1.0$, $k_{-2} = 10^{-4}$, $k_3 = 10.0$, $k_{-3} = 10^{-3}$, $k_4 = 1.0$, $k_{-4} = 10^{-3}$, $k_5 = 16.5$, $k_{-5} = 0.5$. All integrations used the GEAR algorithm (Ref. 21).

the operation of the switch. The details of this study are given in Sec. III.

III. ROUTE TO CHAOS

A. Period doubling

The nonperiodic oscillatory state shown in Fig. 2 is approached via a cascade of period doubling as exemplified by Figs. 4 and 5. In Fig. 4, k_2 is increased from a value where the steady state is stable [Fig. 4(a)]. At this low value of k_2 ($k_2 = 0.7$ vs $k_4 = 1.0$), the LV oscillator dominates the dynamics. Note that the values of k_1 and k_5 (30 and 16.5, respectively) were chosen such that, considering the switch alone, Z is driven to extinction by the faster growing species X. Thus, when k_2 is lower than k_4, X has sufficient time to increase to a level that would consume Z; the trajectories of the network are then attached to the X–Y plane (which we will also refer to as the LV plane). The steady state that is located almost on the LV plane has a one-dimensional unstable manifold and a two-dimensional stable manifold (a spiral). The trajectory shown in Fig. 4(a) is first attracted by the stable spiral, then pulled out by the unstable manifold and finally settles down to a stable steady state inside the positive orthant of concentration space.

A Hopf bifurcation occurs between $k_2 = 0.7$ and 0.8, where the stable steady state mentioned above becomes an unstable spiral and a stable limit cycle is born. In Fig. 4(b), the trajectory is first attracted by the stable manifold of the damped LV oscillator, then repelled by its one-dimensional unstable manifold towards the interior steady state (which has undergone a Hopf bifurcation) from which occurs a very slow approach to the limit cycle. This limit cycle is shown in Fig. 4(c) when all transients are discarded. The amplitude of the limit cycle increases as k_2 is increased, then period doubling occurs near $k_2 = 0.95$, 0.975, etc. [see Figs. 4(d)–4(f)].

In Fig. 5, k_4 is now varied from below and past the value which gives chaos (from 0.6 to 2.0). At $k_4 = 0.6$, the switch is "weakened" so that the stable limit cycle that arises [see Fig. 5(a)] is now distant from the LV plane, i.e., Z is allowed to increase to an appreciable amount during a full oscillation. Period doubling occurs at $k_4 = 0.95$, 0.96 [Figs. 5(b) and 5(c)] until the period approaches infinity and one initial condition fills up the attractor region [Fig. 5(d), at

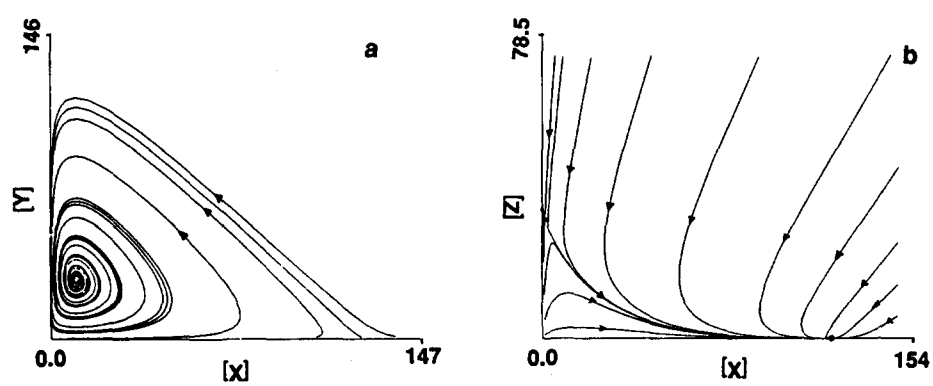

FIG. 3. (a) Damped oscillatory dynamics of the LV element composed of reactions 1, 2, 3 and their reverse. (b) Dynamics of the switch element composed of reactions 1, 4, 5 and their reverse. In (b), there are three steady states—the two that are near the boundary are stable and the third (which is very close to the stable steady state with high Z and almost vanishing X) is an unstable saddle point. (Parameter values as in Fig. 2 for those reactions used.)

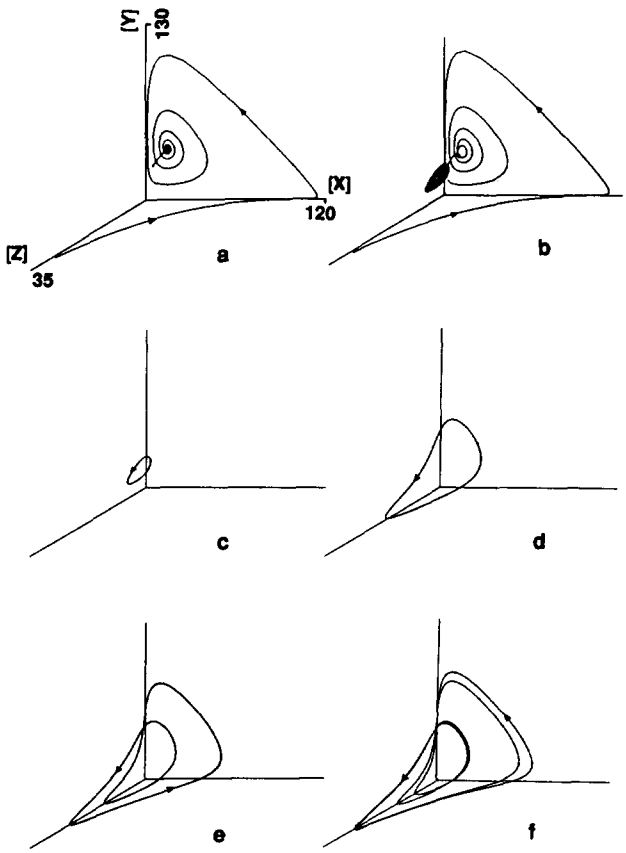

FIG. 4. Dynamics of the WR model when k_2 is varied. (Other parameters are fixed at those values given in Fig. 2.) (a) At $k_2 = 0.7$, the trajectory starting from a high value of Z and almost vanishing X and Y goes through a LV oscillation and then terminates at a stable steady state. (b) At $k_2 = 0.8$, the stable steady state in (a) is now an unstable spiral after undergoing a Hopf bifurcation. A limit cycle is very slowly approached. (c) The limit cycle in (b) after all transients are discarded. The amplitude of the limit cycle has increased at $k_2 = 0.9$ (d) and then undergoes period doubling at $k_2 = 0.95$ (e), $k_2 = 0.975$ (f), etc.

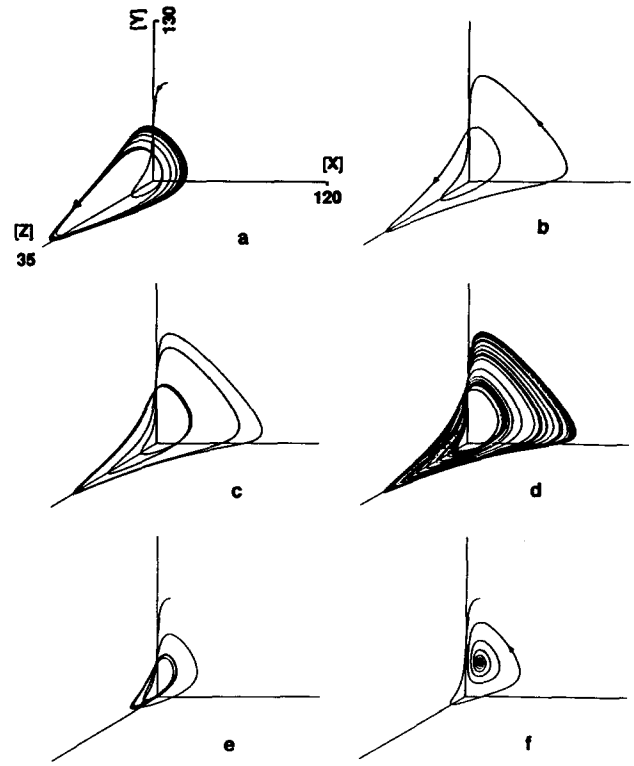

FIG. 5. Dynamics of the WR model when k_4 is varied. (Other parameters are fixed at those values given in Fig. 2.) A stable limit cycle is approached at $k_4 = 0.6$ (a). This limit cycle undergoes period doubling at $k_4 = 0.95$ (b), $k_4 = 0.96$ (c), etc. until the period approaches infinity (nonperiodic) at $k_4 = 0.97$ (d). At $k_4 = 1.3$ (e), the dynamics reverts back to a stable limit cycle, and finally to a stable focus at $k_4 = 2.0$ (f).

$k_4 = 0.97$]. As k_4 is increased further, the effect of the switch is strengthened and, since k_1 is greater than k_5, the trajectories are again shifted to the LV plane [Figs. 5(e) and 5(f)].

B. The chaotic attractor

The structure of the attractor can readily be demonstrated by plotting the intersection points of the trajectories with a series of Poincaré planes that cut through the attractor all around. This is done in Fig. 6. The attractor has a hole in the middle. Four planes perpendicular to the X–Y plane with cross sections shown in Fig. 6 by the line segments a–d were used and the different Poincaré sections of the attractor are shown.

The attractor exists within a range of parameters and undergoes a continuous change in structure. The left column of Fig. 7 shows how the cross section of the attractor changes as k_5 is varied. The number of foliations increases as k_5 is increased from 16.42 to 16.58. Beyond $k_5 = 16.6$, the system eventually settles into a stable steady state but only after undergoing a very long chaotic transient whose flow has a Poincaré section similar, although not filled up, to Fig. 7(d).

Using a Poincaré line like Fig. 6(b), the corresponding first-return maps are shown at the right column of Fig. 7. The topological equivalence of these two sets of curves (left and right columns of Fig. 7) is obvious and expected.[15] Note that there is one unstable fixed point of the map at $k_5 = 16{,}42$, two at $k_5 = 16.47$, and three at $k_5 = 16.55$. Since the slope of the curves at these fixed points have magnitudes greater than unity, all the fixed points are unstable.

C. Proof of chaos

A first proof of the chaotic nature of the trajectories is to look for period 3 fixed points of the return maps. According to the Li–Yorke theorem,[16] the existence of period 3 implies that there exists an infinite number of periodic solutions and an uncountable number of nonperiodic solutions. Figure 8 shows the third-iterate map for three different values of k_5 [also used in Figs. 7(a)–7(c)].

The increase in k_5 from 16.42 to 16.55 is accompanied by the increase in the number of unstable period 3 fixed points: one at $k_5 = 16.42$, ten at $k_5 = 16.47$ and at $k_5 = 16.55$ the system is on the verge of having 12. Tangent bifurcations creating some of these period 3 fixed pints are indicated by Figs. 8(b) and 8(c).

We have discovered further that the system satisfies the requirements of the Shil'nikov theorem[14] which is discussed next.

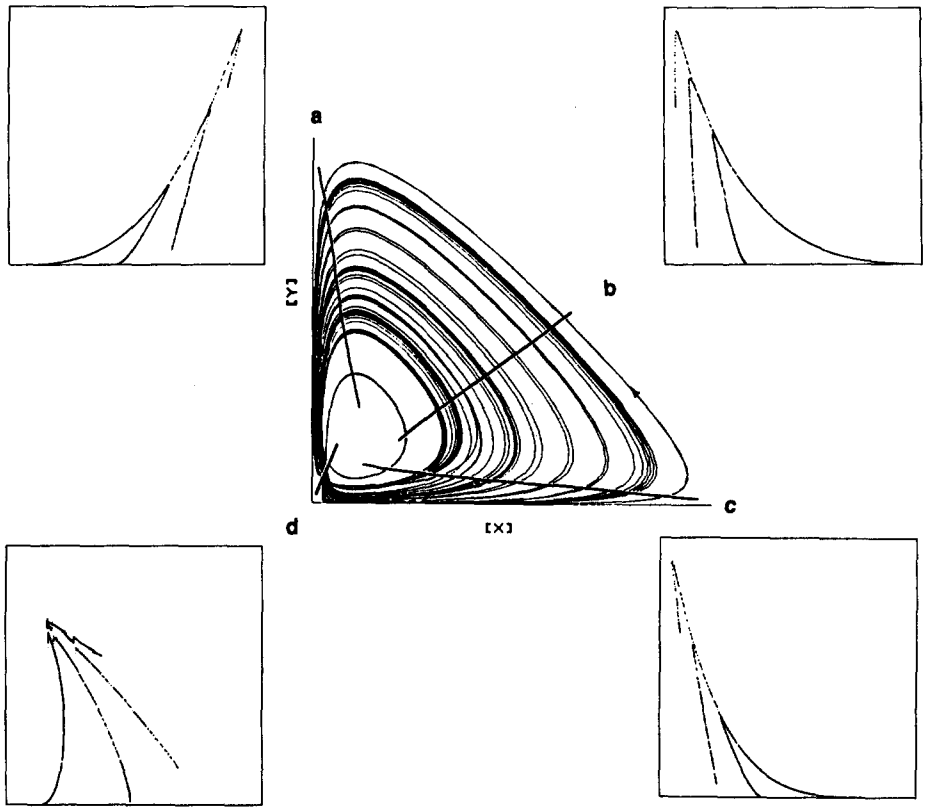

FIG. 6. Poincaré sections of the chaotic attractor. Four planes perpendicular to the X–Y plane and towards the positive Z direction cut through the attractor at the positions indicated by line segments a–d. The corresponding Poincaré sections are shown adjacent to each of these line segments. (All parameter values as in Fig. 2 except $k_5 = 16.58$.)

IV. HOMOCLINIC ORBITS AND THE SHIL'NIKOV THEOREM

At the parameter values where chaos is observed, two steady states of the network were found: one almost at the X–Y plane (or LV plane) and the other well within the positive orthant of concentration space. We shall refer to the first steady state as SSI and the second as SSII. In Fig. 9(a), the trajectory is started very near SSII which is clearly shown to be a saddle focus with a two-dimensional unstable spiral and a one-dimensional stable manifold. The trajectory shown is the closest approximation of the homoclinic orbit that presumably exists at or near the parameters used in the figure. This structurally unstable orbit is doubly asymptotic to the steady state SSII as time approaches positive or negative infinity. The presence of this homoclinic orbit confirms the chaotic nature of the oscillations as will be discussed below using a remarkable result due to Shil'nikov.[14] In Fig. 9(b), the trajectory is started near steady state SSI. This figure confirms our linear stability analysis about this steady state which predicts that it is a saddle focus but now the two-dimensional spiral is stable and the one-dimensional manifold is unstable.

A fundamental step in the study of stochasticity in ordinary differential equations is showing the existence of infinitely many isolated periodic orbits.[17] The relevance of homoclinic orbits to the existence of infinitely many periodic orbits is the subject of the Shil'nikov theorem. The following statement of the theorem is due to Ref. 14.

A. The Shil'nikov theorem

Consider the three-variable system

$$\begin{aligned} \dot{x} &= ax - by + P(x, y, z), \\ \dot{y} &= bx + ay + Q(x, y, z), \\ \dot{z} &= cz + R(x, y, z), \end{aligned} \tag{2}$$

where P, Q, and R are analytic functions vanishing together with their first derivatives at the origin (0, 0, 0) which is a saddle focus. Assume that one of the orbits, T_0, leaving the saddle focus returns to it as t approaches infinity. Then

(i) if $c > -a > 0$ (or if $-c > a > 0$) then every neighborhood of T_0 contains a countable set of unstable periodic solutions of the saddle type; and

(ii) there exists in a neighborhood of T_0 a subsystem of trajectories which display random behavior in the sense that they are in one-to-one correspondence with a shift automorphism with an infinite number of symbols.

Note that the origin is a steady state of system (2). The eigenvalues of the Jacobian matrix evaluated at the origin are c and $a \pm bi$. Thus condition (i) of the theorem corresponds to a saddle focus whose trajectories on the two-dimensional eigenspace are slower than those along the one-dimensional eigenspace.

At the values of the parameters used in Fig. 9, the eigenvalues associated with SSI are $+6.497$ and $-1.2556 \pm 16.596i$ while those of SSII are -12.473 and $+1.735 \pm 8.578i$. Thus both steady states satisfy condition (i) of the theorem. We expect that there is also a homoclinic

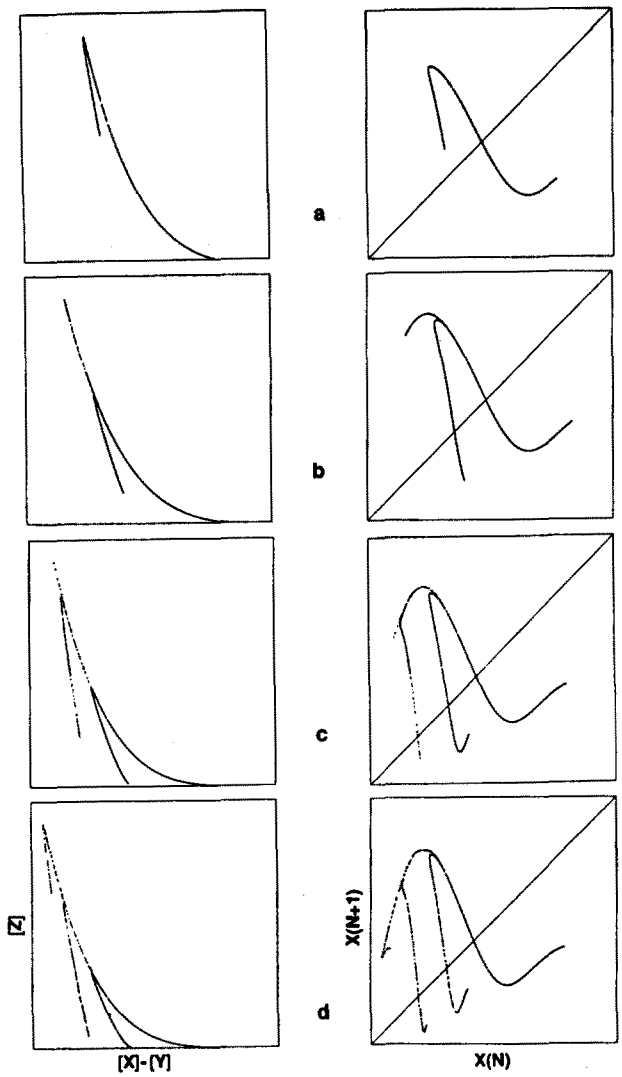

FIG. 7. Poincaré sections of the chaotic attractor (left column) and corresponding first-return maps (right column) as k_5 is varied. (All other parameter values as in Fig. 2.) The Poincaré plane is situated as in Fig. 6(b). Values of k_5: (a) 16.42, (b) 16.47, (c) 16.55, (d) 16.58.

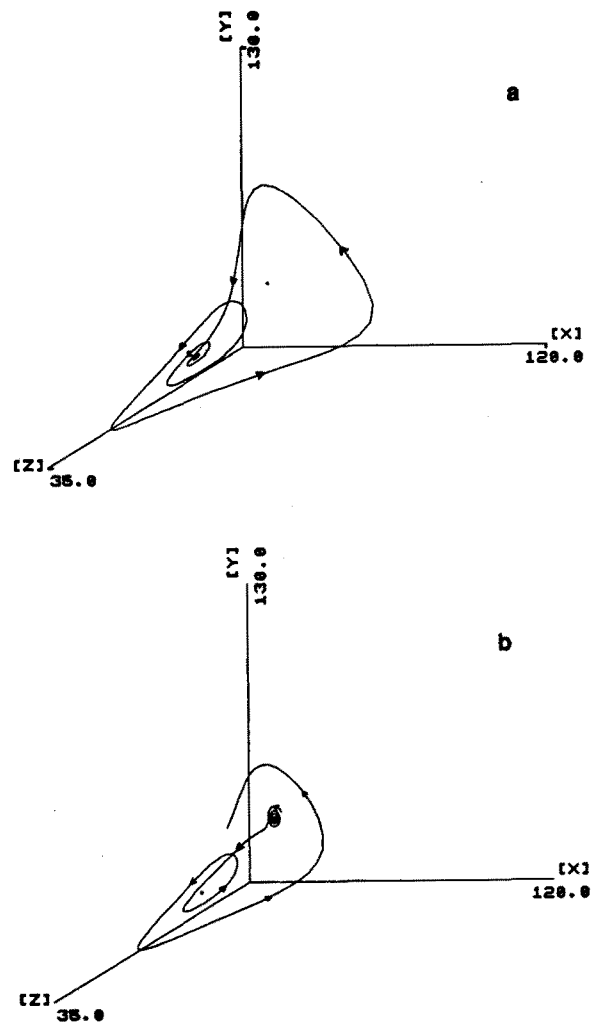

FIG. 9. Trajectories starting very close to the two steady states (shown by solid dots) of the WR model at $k_1 = 30.2$ (all other parameter values as in Fig. 2). (a) A close approximation of the homoclinic orbit doubly asymptotic to the steady state with a two-dimensional unstable spiral. (b) Trajectory started near the steady state that is almost on the X–Y plane, has a two-dimensional stable spiral and a one-dimensional unstable direction.

orbit associated with SSI near the parameter values where such an orbit is found for SSII. The approximate structure of this second homoclinic orbit can be deduced from Fig. 9(b). Gaspard and Nicolis[14] have analyzed another Rössler model[18] and found a very similar situation—two steady states, both saddle foci, and each with an associated homoclinic orbit existing at different parameter values.

V. CONCLUDING REMARKS

We have highlighted through detailed numerical simulations the coupling of two dynamic elements—a switch and an LV oscillator—which leads to chaotic oscillations for some parameter values. The flow of the trajectories in concentration space can now be understood intuitively in terms

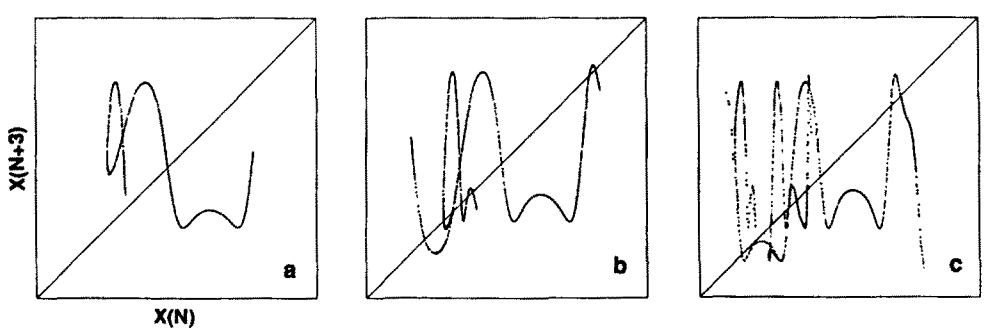

FIG. 8. Third-iterate maps at different values of k_5: (a) 16.42, (b) 16.47, (c) 16.55. (All other parameter values as in Fig. 2.)

of these dynamic elements. Starting at a high value of X and a very low value of Z, the trajectory goes through a large amplitude Lotka–Volterra oscillation until X attains a low enough concentration that the switch (which tends to extinguish Z) cannot operate, and thus allows the autocatalytic species Z to increase. The trajectory is driven towards increasing Z until a point where the switch is again fully activated and causes Z to decrease with a concomitant increase in X. Notice here that it is necessary that X autocatalyzes faster than Z (i.e., $k_1 > k_5$) otherwise Z would consume all X thereby rendering the LV oscillator inoperative.

The nonperiodic oscillations shown by the model can be considered to be of the screw type.[12] As was also observed in another study,[14] the appearance of the foliation in the first-return maps indicate the transition to a screw-type chaos. Although there is no hysteresis between two stable limit cycles in the WR model, the same principle of generating chaos is followed by the switching of the trajectories between the stable spiral (the two-dimensional manifold of steady state SSI near the LV plane) and the unstable spiral (the two-dimensional unstable manifold of steady state SSII) as demonstrated in Fig. 9. The switch between these two spiral manifolds is effected by the one-dimensional unstable manifold of steady state SSI as clearly shown in Figs. 4(a), 4(b), and 9(b). The region in concentration space where these two spiral manifolds most overlap is near the origin [see Fig. 6(d)]. Here the trajectories are very sensitive to initial conditions.

Rössler's very intuitive construction of chaotic model networks represents success in the understanding and predicting complex dynamics by identifying the dynamic elements comprising a large network. Nevertheless, it is also very important to come up with practical computational criteria as to when a dynamical system is about to become chaotic. The difficulty in predicting a transition to chaos mainly lies in the fact that this phenomenon is global in character and linearization techniques do not apply. However, a promising approach has come from the observation that many transitions which are global when one control parameter is varied become local when more than one such parameters are considered. Indeed, it has been shown that complex nonperiodic behavior already occurs near certain codimension-two bifurcation points.[19]

The requirements of the Shil'nikov theorem on the eigenvalues of the linearized dynamics has also given us a good reason for looking at codimension-two bifurcation points. Chaos in the WR network was first thought to occur near a codimension-two bifurcation point that involves three eigenvalues simultaneously crossing the imaginary axis of the Argand diagram (i.e., one zero real eigenvalue and a pair of conjugate pure imaginary eigenvalues). Perturbation of this degenerate case can lead to the Shil'nikov requirement on the eigenvalues.

Using the parameters of stoichiometric network analysis (SNA), we have shown[20] that the above type of codimension-two bifurcation point is impossible for any set of positive rate constants. We have not discounted, however, the possibility that this bifurcation may occur when negative rate constants are allowed.

Condition (i) of the Shil'nikov theorem can also be satisfied after a perturbation of a codimension-two bifurcation point where all three eigenvalues are real and two of these are zero simultaneously. These two then become a pair of complex conjugate eigenvalues after a bifurcation. Indeed, using SNA parameters, we have shown[20] that there exist parameters where two eigenvalues are zero at the same time (the other eigenvalue being always negative). These conclusions cannot be derived if one directly uses the usual rate constants as parameters. The details of these analytic results will be presented in a later paper.

[1] A. J. Lotka, J. Phys. Chem. **14**, 217 (1910).
[2] L. F. Olsen, Phys. Lett. A **94**, 454 (1983).
[3] B. D. Aguda and R. Larter (in preparation).
[4] A. J. Lotka, J. Am. Chem. Soc. **42**, 1595 (1920).
[5] R. Lefever and G. Nicolis, J. Theor. Biol. **30**, 267 (1971).
[6] I. R. Epstein, Chem. Eng. News XX (1987).
[7] (a) J. Boissonade and P. De Kepper, J. Phys. Chem. **84**, 501 (1980); (b) P. De Kepper, K. Kustin, and I. R. Epstein, J. Chem. Soc. **103**, 2133 (1981); (c) I. R. Epstein, K. Kustin, P. De Kepper, and M. Orban, Sci. Am. **248** (3), 112 (1983).
[8] B. D. Aguda and B. L. Clarke, J. Chem. Phys. **87**, 3461 (1987).
[9] L. J. Aarons and B. F. Gray, Chem. Soc. Rev. **5**, 359 (1976).
[10] B. L. Clarke, Adv. Chem. Phys. **43**, 1 (1980).
[11] O. E. Rössler, Z. Naturforsch. Teil A **31**, 259 (1976).
[12] O. E. Rössler, Bull. Math. Biol. **39**, 275 (1977).
[13] K.-D. Willamowski and O. E. Rössler, Z. Naturforsch. Teil A **35**, 317 (1980).
[14] P. Gaspard and G. Nicolis, J. Stat. Phys. **31**, 499 (1983).
[15] N. H. Packard, J. P. Crutchfield, J. D. Farmer, and R. S. Shaw, Phys. Rev. Lett. **45**, 712 (1980).
[16] T. Y. Li and J. A. Yorke, Am. Math. Monthly **82**, 985 (1975).
[17] A. Arneodo, P. Coullet, and C. Tresser, J. Stat. Phys. **27**, 171 (1982).
[18] O. E. Rössler, Ann. N. Y. Acad. Sci. **316**, 376 (1979).
[19] C. Baesens and G. Nicolis, Z. Phys. B **52**, 345 (1983).
[20] B. D. Aguda and B. L. Clarke (unpublished).
[21] A. C. Hindmarsh, GEAR: Ordinary Differential Equation Systems Solver, UCID-30001 Rev. 3, Lawrence Livermore Laboratory, December, 1974.